EXPERIMENTAL AND NUMERICAL STUDIES OF SINGLE-PHASE HEAT TRANSFER ENHANCEMENT IN A TUBE

S. Doerffer[a], A.O. Banas[a] and C.H. Wang[b]

[a]Fuel Channel Thermalhydraulics Branch
AECL
Chalk River Laboratories
Chalk River, Ontario
K0J 1J0

[b]Visiting NSERC Fellow

ABSTRACT

Fuel-element appendages affect the thermalhydraulic performance of a CANDU fuel channel by increasing its pressure drop and enhancing fuel-to-coolant heat transfer. The high cost of characterization of these effects through experiments provides incentive to develop reliable numerical methodologies by which to quantify relevant parametric trends. Recent studies at Chalk River Laboratories indicate that the current capabilities of Computational Fluid Dynamics (CFD) are adequate to assess the fuel-appendage effects under normal operating (single-phase) conditions from simulations alone. This paper describes the experimental work undertaken to provide data for validation of CFD models used in the numerical assessment of appendage effects, and presents preliminary results of a validation study completed with the TASCflow software.

Heat transfer and pressure drop in single-phase flow through a vertical pipe obstructed by a cylindrical ring were investigated experimentally in the MR-7A loop at Chalk River Laboratories using Freon-134a as a coolant. The test section was a vertical 8 mm ID directly heated tube, made of Inconel 600. Two ring-shaped flow obstructions were tested; they reduced the flow area by 17.8% and 30%. The presence of the flow obstructions enhanced heat transfer up to 38% and 61%, respectively. These significant changes were observed in the downstream region, over a very short distance behind the obstruction. The tests were carried out within the mass flux range between 1 and 6 Mg/m^2s, and the highest relative heat-transfer enhancement occurred at 1 Mg/m^2s. The pressure drop increase due to the flow obstructions was characterized by the form loss factor, K, which was found to be 0.18 and 0.45, for the 17.8% and 30% rings, respectively.

The heat-transfer enhancement and pressure-drop experiments were subsequently simulated numerically using TASCflow software. All simulations were performed assuming axisymmetric flow conditions, and employing the "standard" k–ϵ model for turbulent flows. Forced convection in Freon and conjugated heat conduction in the ring and the tube walls were modelled. The predictions generated by the code agreed well with the experimental results for both heat transfer and pressure drop. This demonstrates the merit of using computational, CFD-based methodology to assess appendage effects in single-phase forced convection flows.

1 INTRODUCTION

CANDU* fuel channels use bearing pads and spacers to maintain, respectively, the bundle separation from the pressure tube, and the separation of the fuel elements from each other. These appendages significantly affect pressure drop and heat transfer in single-phase flow under normal operating conditions, and can increase channel dryout power. The high cost of characterizing these effects through experiments provides incentive to develop reliable prediction methodologies by which to quantify relevant parametric trends. Recent studies at Chalk River Laboratories (CRL) [1, 2] indicate that the current capabilities of Computational Fluid Dynamics (CFD) are adequate to simulate realistic single-phase flow and temperature fields around fuel-element appendages, and provide plausible predictions of pressure drop and heat-transfer enhancement under normal operating conditions. To qualify the CFD tools to predict the effects of such appendages, systematic experimental and numerical investigations are required to establish that simulations reproduce the measurement data with sufficient accuracy for various appendage configurations and over a range of power and flow conditions.

Previous numerical simulations of local hydrodynamics and heat transfer in obstructed channels employed two commercial CFD software packages, CFDS-FLOW3D† [3] and TASCflow‡ [4]. They established a proof-of-concept for CFD-based prediction methodologies, but lacked experimental validation. To address this concern, an experimental program was launched to provide a data base for systematic validation of TASCflow models of turbulence and heat transfer over the range of Reynolds numbers of relevance to CANDU-channel operating conditions. The results of the validation study confirm that TASCflow can be used with confidence to predict the appendage effects on pressure drop and heat transfer in channel geometries.

2 EXPERIMENTAL STUDY

To investigate the effects of flow obstruction on heat transfer and pressure drop, a special experimental test section was designed and accommodated in the MR-7A multi-fluid loop at CRL. The facility, test section, instrumentation, and main heat-transfer and pressure-drop results are briefly described and illustrated in the following sections.

2.1 Facility

In the MR-7A loop, a working fluid (Freon-134a in the present tests) flows through two magnetically driven gear pumps connected in series, an electric preheater and a test section; it then flows through a condenser and a subcooler back to the pump inlet. The pressure in the test section can be changed by changing pressure in the pressurizer, which is connected to the loop at the pump outlet. The loop and the test section are equipped with all necessary instrumentation to measure: mass flow rate, absolute pressure, pressure drop across the test section, power input to the test section, fluid and test-section wall temperatures. The measurements are recorded by an on-line data acquisition system (DAS). By appropriate selection of the absolute pressure, inlet temperature, mass flow rate and power values, the working fluid can be maintained in a state of single phase in the test section.

*CANDU: CANada Deuterium Uranium. Registered Trademark.

†CFDS-FLOW3D is a Registered Trademark of AEA Technologies.

‡TASCflow is a Registered Trademark of Advanced Scientific Computing Ltd.

2.2 Test Section

The test section was situated vertically, as shown schematically in Figure 1 (see Nomenclature at the end of the paper). It consisted of an 8 mm ID round tube made of Inconel 600 with 1 mm wall thickness; its total length was about 3 m, while the heated part was 2.05 m long. This part was resistance-heated by a DC current generated by a 50 kW power supply. To minimize the heat loss from the test section to the surrounding area, rubber foam insulation was used.

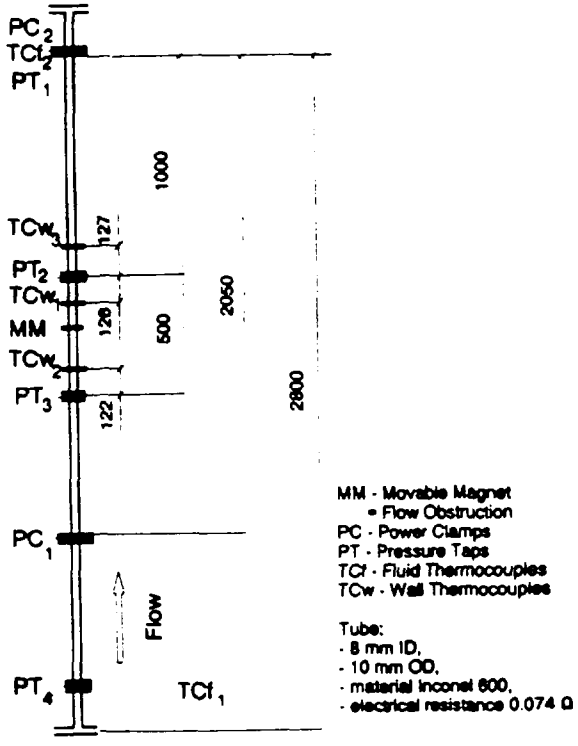

Figure 1: Test Section

2.3 Instrumentation

The fluid temperatures at the inlet and outlet of the test section were measured using thermocouples. The outer-wall temperatures were recorded by eight wall thermocouples placed in three movable (and demountable) clamps, in sets of three, three and two (*i.e.*, TCw_1, TCw_2 and TCw_3, respectively). To improve the accuracy of the wall-temperature measurements, these thermocouples were insulated with special Teflon sheaths, and special copper tips were attached to the thermocouples' junctions to improve their thermal contact with the tube wall.

The absolute pressure at the test section outlet was measured at pressure tap PT_1 by a pressure transducer. Pressure taps PT_1 and PT_4 were also connected to a pressure-differential transducer, to measure the total pressure drop along the test section, while taps PT_2 and PT_3 were connected to an additional pressure-differential transducer, to accurately measure the pressure drop across the flow obstruction.

The mass flow rate was measured using a Coriolis-type flow meter. The power supplied to the test section was determined from the measurements of voltage drops along the heated length and across a calibrated shunt. The latter measurement permitted an easy calculation of the current passed through the test section.

2.4 Flow Obstructions

The first series of experiments were performed using a ring of rectangular cross-section (*i.e.*, a short hollow cylinder) that obstructed the flow area by 17.8%. To produce more pronounced effects, the next series of experiments used another ring that obstructed the flow area by 30%. Both rings were 6.5 mm long, and their wall thicknesses were 0.35 mm and 0.65 mm, respectively.

A new technology was developed to relocate the flow-obstructing ring inside the tube during heat-transfer experiments. The ring was held in place by an external magnet, and was repositioned by moving the magnet axially along the tube. Relocating the flow obstruction rather than the thermocouples themselves assured more accurate results, as the thermocouples' contact resistances were not changed during the operation. In addition, this new technology reduced the number of thermocouple planes required, and simplified the measurements. Figure 2 shows the cross-section of the obstruction ring and the axial locations at which it was tested.

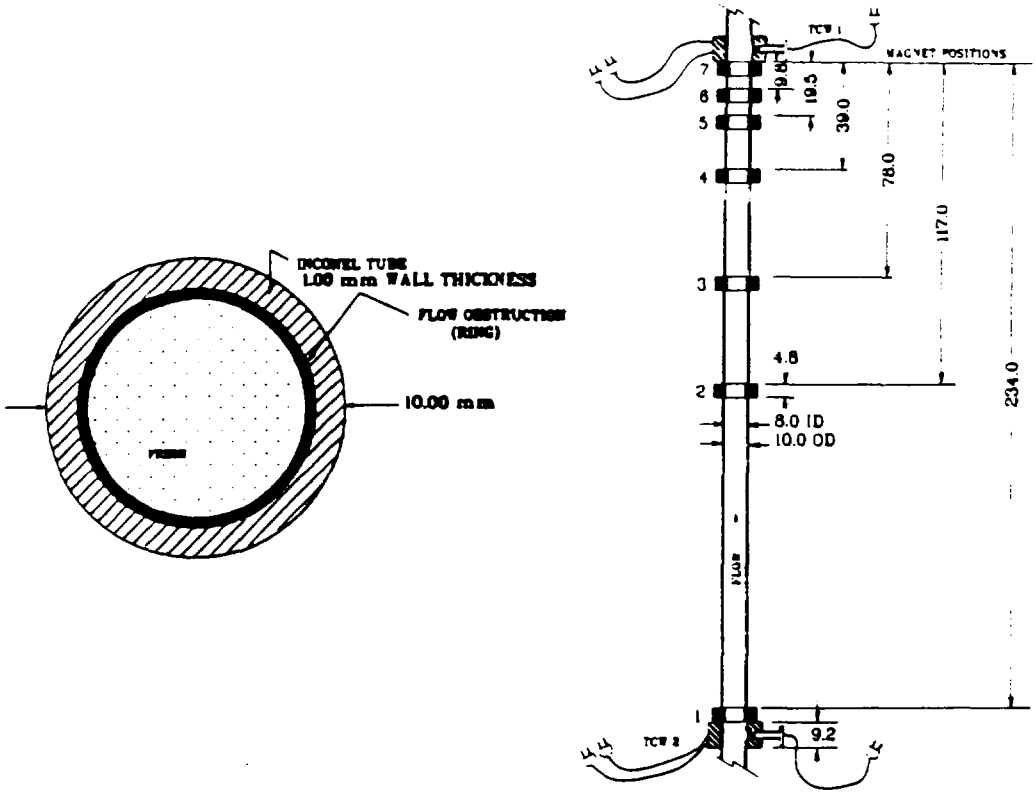

Figure 2: Cross-Section of Obstruction Ring and Its Axial Locations

2.5 Test Procedure

Before applying power to the test section, the required flow conditions were established as follows:

- the mass flux was set approximately to the required value by adjusting the rotation speed of the pumps,
- the pressure at the test-section outlet was set in the range between 1.8 and 1.9 MPa, and was controlled by the pressurizer, and
- the inlet fluid temperature was set and controlled by the preheaters and the flow in the subcooler.

Subsequently, the test-section power was turned on and increased gradually to reach the required value. The mass-flow rate, pressure and inlet temperature were monitored and, if necessary, adjusted to maintain a steady state corresponding to specified conditions.

Once the steady state was reached, the data were recorded by the DAS as a set of time-averaged values from six consecutive scans. To ensure the repeatability of the results, the data were recorded at least five times at few-minutes intervals. For the same power and flow conditions, the measurements were taken at seven axial locations of the flow obstruction (see Figure 2).

The procedure was repeated until all planned runs were completed. The test matrix is listed in Table 1. This matrix was arranged to simulate the operating conditions of CANDU reactors as closely as possible. The CANDU conditions correspond to the Reynolds number range, $Re = 2.8 \times 10^5$ to $Re = 5.6 \times 10^5$, and the Nusselt number range, $Nu = 500$ to $Nu = 860$. During the tests, the Nusselt number range was fully covered, while the maximum $Re = 2.4 \times 10^5$ was imposed by loop limitations.

Table 1: Test Matrix

Ring	17.8% Flow Obstruction Area				30% Flow Obstruction Area				
Power, P [kW]	4	7	12	15	4	6	8	15	20
Mass Flux, G [kg/m^{2}s]	1000	2000	4000	6000	1000	1500	2000	4000	6000
Inlet Temperature, $T_{bf,in}$ [°C]	3	3	7	10	3	3	7	10	10

2.6 Heat-Transfer Results

The flow obstruction affected the heat transfer, and resulted in changes in the wall temperature. The changes at the wall's outer surface were measured using the thermocouples TCw_1 to observe the downstream effect, and using the thermocouples TCw_2 to observe the upstream effect. As mentioned earlier, these thermocouples remained at the same respective locations during all tests, to maintain the same thermal contact with the wall.

Figures 3 and 4 illustrate the dependendence of outer-wall temperature, $T_{wo,1}$, on the relative axial distance, L/D_i (where L is measured from the downstream face of the obstruction), and on mass flux, G. This temperature is an arithmetic average of the values around the tube perimeter, taken from readings of all thermocouples at the TCw_1 location.

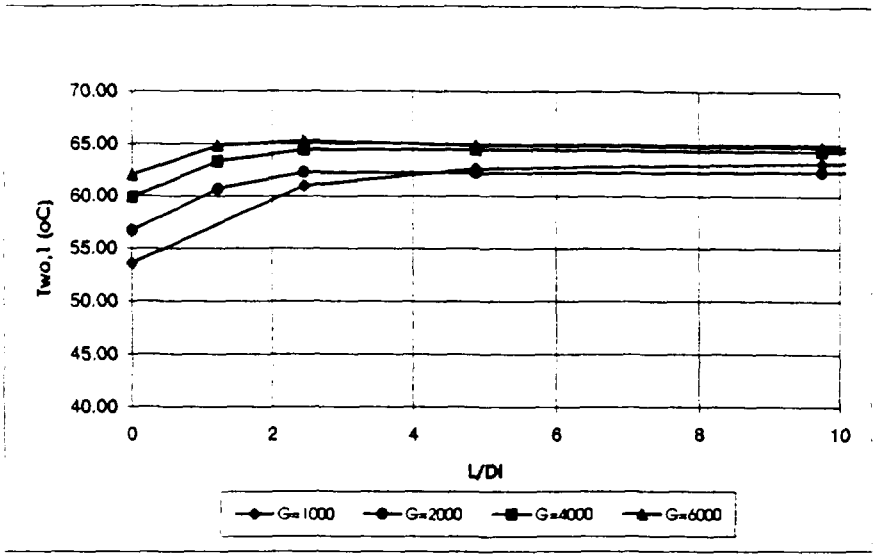

Figure 3: Wall-Temperature Changes at TCw_1 for 17.8%-Obstruction Ring

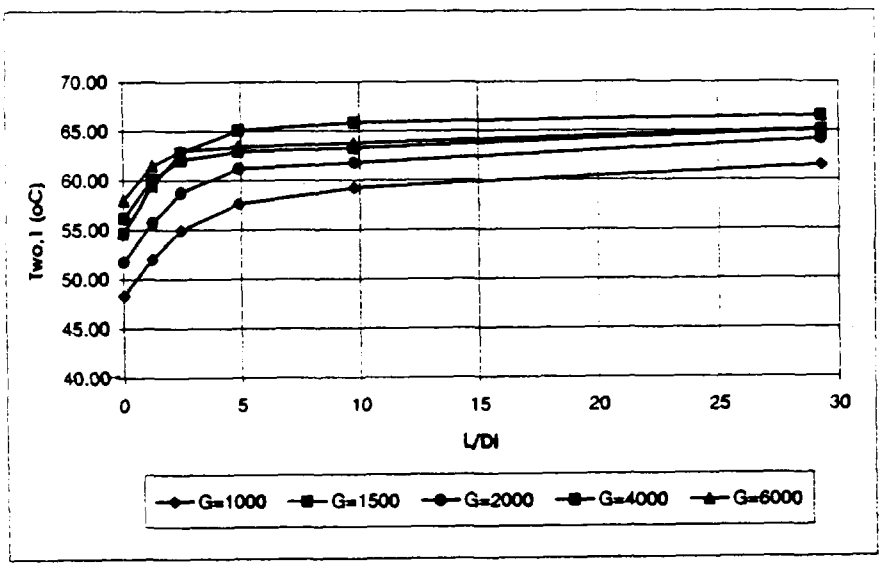

Figure 4: Wall-Temperature Changes at TCw_1 for 30%-Obstruction Ring

The largest temperature changes, $\Delta T_{wo,1}$, (*i.e.*, when the ring was moved from position 1 to 7) were as follows:

- For the ring with 17.8% of the flow-area reduction:
  1. $\Delta T_{wo,1} = 9.9°C$ at $G = 1000\,kg/m^2s$, $P = 4\,kW$ and $T_{bf,in} = 3°C$, and
  2. $\Delta T_{wo,1} = 2.6°C$ at $G = 6000\,kg/m^2s$, $P = 15\,kW$ and $T_{bf,in} = 10°C$. The axial effect was extended to $L/D_i \approx 5$.
- Similarly, for the ring with 30% of the flow-area reduction ring:
  1. $\Delta T_{wo,1} = 11.9°C$ at $G = 1000\,kg/m^2s$, $P = 4\,kW$ and $T_{bf,in} = 3°C$, and
  2. $\Delta T_{wo,1} = 7.2°C$ at $G = 6000\,kg/m^2s$, $P = 16\,kW$ and $T_{bf,in} = 10°C$. The axial effect extended up to $L/D_i \approx 10$.

No significant effect on the upstream wall temperature was observed in either case.

2.7 Pressure-Drop Results

The pressure-drop data were obtained in both adiabatic and diabatic conditions. The examples of the reference data (without flow obstruction) and the data obtained with the 17.8% and 30% flow-area obstruction are shown in Figure 5 as functions of mass flux (for fluid temperature in the range between 23°C and 26°C at position TCw_1).

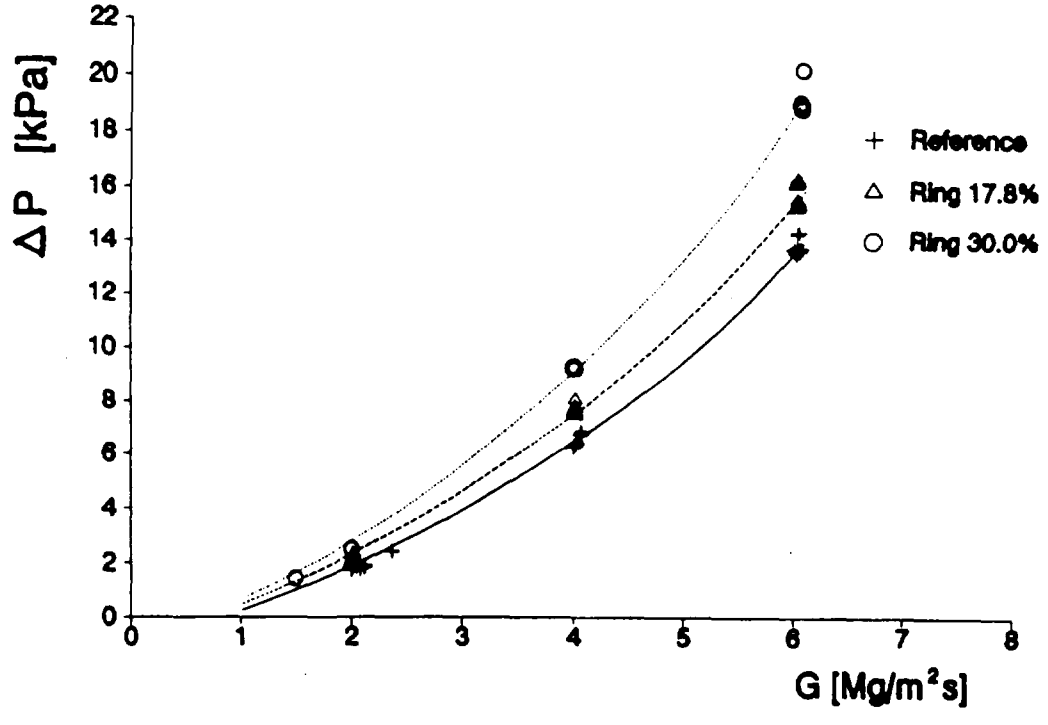

Figure 5: Pressure Drops Measured over the Distance of 0.5 m for Bare and Obstructed Channels

The pressure-recovery region downstream of the obstructions was probably quite short, because no changes in the pressure drop were observed, regardless of the obstruction location between taps PT_2 and PT_3.

The reference pressure-drop data were compared with a standard pressure drop equation for bare tubes:

$$\Delta p_{unobst} = f \frac{L}{D_i} \frac{G^2}{2\rho}, \tag{1}$$

using the Prandtl formula to assess the Fanning friction factor, f,

$$\frac{1}{\sqrt{\Lambda}} = 2.0 \log (Re_D \sqrt{\Lambda}) - 0.8, \tag{2}$$

where the Moody-Weisbach friction factor is defined as:

$$\Lambda = 4f, \tag{3}$$

which is valid for smooth-wall turbulent pipe flow ($Re_D > 4 \times 10^3$).

The discrepancies between the experimental and predicted values were found to be within $\pm 10\%$ for $Re > 10^5$ or $G > 2000\,\mathrm{kg/m^2s}$.

Pressure drop induced by flow obstruction was used to calculate the *form-loss coefficient* (usually referred to as the *K–factor*) for a given ring as follows:

$$K = \frac{\Delta p_{obst}}{\frac{1}{2}\frac{G^2}{\rho}}, \tag{4}$$

where the pressure drop across the obstruction was calculated as the difference between the total pressure drops measured with and without the obstruction:

$$\Delta p_{obst} = \Delta p_{tot,obst} - \Delta p_{unobst}. \tag{5}$$

A correlation based on the reference data was used as a basis for an assessment of Δp_{obst} and for a subsequent K determination at the same Reynolds number. It was found that:

- for the 17.8%–obstruction ring, $K \approx 0.18$, and
- for the 30.0%–obstruction ring, $K \approx 0.45$.

These measurements agree with the literature data (*e.g.*, [5]) for the turbulent flow regime (*i.e.*, for $Re > 10^5$). The maximum error in Δp_{obst} measurements was $\pm 1.8\%$, while the error in the K assessment was $\pm 15.3\%$ and $\pm 12\%$, for 7.9%– and 30%–obstruction rings, respectively.

3 NUMERICAL STUDIES

3.1 TASCFLOW Software and Its Models

TASCflow [4] is an integrated CFD software package, developed and distributed by Advanced Scientific Computing Ltd. (ASC). The main component of the package is the flow solver, which uses an advanced finite-volume methodology to discretize and numerically solve the coupled mass- and momentum-transport equations, complemented if necessary by the energy transport equation, for viscous (incompressible or compressible) fluids in arbitrary three-dimensional geometries. Separate modules exist for grid generation, specification of boundary conditions and material properties, and for post-processing and visualization. Options are available for discretization schemes, to devise iterative solution strategies, and to invoke special models.

The validation study reported in this paper used two important modelling options in TASCflow; the k–ϵ model of turbulence transport, as originally developed by Launder and Spalding [6], was used to represent the effects of high–Re turbulence on the mean flow, and the *conjugated heat transfer* option was invoked to couple the solution of the heat-conduction problem in the pipe wall and obstruction ring with the convective heat-transfer problem for Freon.

The k–ϵ model appends two additional scalars, the *turbulent kinetic energy*, k, and the *turbulent energy dissipation*, ϵ, to the set of mean-flow variables (velocity components, pressure and temperature). The modelled k– and ϵ–transport equations are solved, along with the mean-flow transport equations, at every grid point, and their values provide local estimates of *eddy* (or *turbulent*) *viscosity*, μ_t, and *turbulent thermal diffusivity*, γ_t:

$$\mu_t = \frac{C_\mu \rho k^2}{\epsilon}, \tag{6}$$

$$\gamma_t = \frac{\mu_t}{Pr_t}. \tag{7}$$

The turbulent viscosity and thermal diffusivity are fed back into the mean-flow equations to constitute the Reynolds stresses and turbulent energy flux, respectively. The empirical constants in Eqs. (6) and (7) are assigned the "standard" values, $C_\mu = 0.09$ and $Pr_t = 0.9$. The k- and ϵ-transport equations involve additional empirical constants that form an inherent part of the phenomenological turbulence model. However, these equations are not valid near solid boundaries, and cannot be integrated in their vicinity. In TASCflow, a semi-empirical *wall-function treatment* based on the development of Launder and Spalding [6] is used to model the turbulent behaviour in the control volumes adjacent to the solid walls. In the studies reported in this paper, the recommended default values of all the wall-function constants were used, as required by the standard k-ϵ turbulence model (for hydraulically smooth walls).

The conjugated heat-transfer computation introduces the coupling between solid conduction and fluid convection through the enforcement of interfacial continuity for both temperature and heat flux. In effect, this treatment allows for the unconstrained settling of temperature fields across the entire computational domain, and the variations of both temperature and heat flux along all fluid-solid interfaces are computed as part of the overall solution. The main advantage of the coupled formulation is that it frees the user from specifying the heat-transfer coefficient at the internal solid-fluid interfaces.

3.2 Computational Domain and Grid Generation

In the validation studies discussed in this paper, the selection of the computational domain was dictated by two considerations. First, the flow through the vertical test section described in section 2.1 was assumed to be perfectly axisymmetric (without swirl), and this axisymmetry was assumed to carry over to the heating conditions. Under this assumption of two-dimensionality, the computational domain could be selected in the shape of a cylinder sector, representing the $r-z$ cross-sectional plane in the cylindrical coordinate system. The second issue considered was the minimum extent of the computational domain in the axial z–direction. The model included the 2050 mm-long heated portion of the channel (see Figure 1); an additional 200 mm of unheated length was added upstream, to ensure that hydrodynamically developed flow was always computed at the entrance to the heated section.

The TASCgrid program was used to generate the grid of finite volumes distributed over the selected domain. The grid generation task involved a sequence of steps: (1) division of the domain into rectangular regions; (2) distribution of nodes along edges of individual regions; (3) distribution of nodes along boundary surfaces; and (4) meshing the interiors of all regions. In total, $130 \times 8 \times 13$ finite volumes were used to represent the pipe wall, the ring and the fluid parts of the computational domain. For computational expediency, the volumes were distributed non-uniformly, as illustrated in Figure 6.

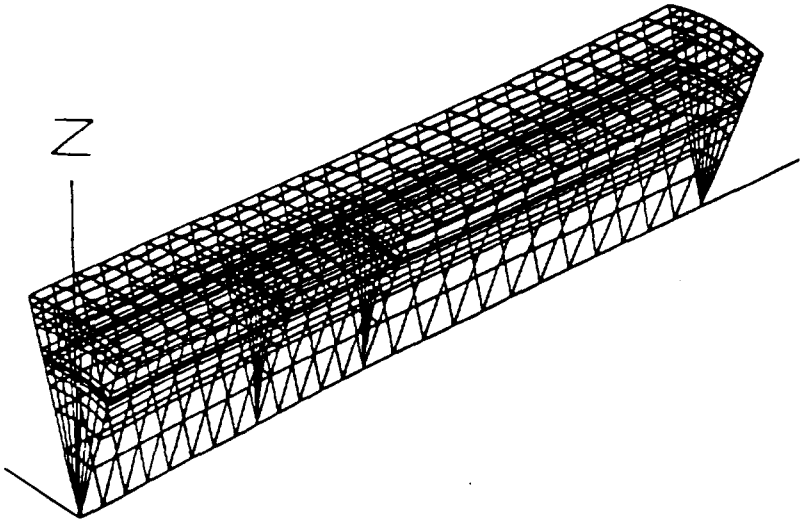

Figure 6: Surface Node Distribution over the Part of the Domain Containing Obstruction Ring

3.3 Modelling Assumptions and Boundary Conditions

In addition to previously outlined modelling considerations, the following simplifying assumptions were invoked in constructing the TASCflow model:

- Freon-134a was considered an incompressible fluid of constant thermophysical properties (evaluated at channel-inlet conditions); consequently, any effects of buoyant forces (variable density) on turbulence generation and temperature distribution were neglected;
- pipe and ring materials were assumed to be rigid conductors characterized by constant values of thermal conductivity;
- electrical heating was assumed to result in a uniform volumetric heat generation within the pipe material, but no heat generation in the ring volume;
- thermal contact resistance at the solid-solid interface (between the pipe wall and the obstruction ring) was assumed to be negligible.

The following hydrodynamic and thermal boundary conditions were specified to complete the model:

- the turbulent-wall functions, appropriate for smooth solid surfaces, were invoked to approximate the near-wall behaviour of fluid velocities, turbulent quantities and temperature;
- mass-flow rates and uniform temperature profiles were specified at the channel inlet, according to measurements;
- the inlet values of k and ϵ were assigned in accordance with empirical guidelines, considered valid for most industrial flows:

$$k_{in} = \frac{3}{2}\rho\,(0.05\,U_{in})^2, \tag{8}$$

$$\epsilon_{in} = \frac{{k_{in}}^{\frac{3}{2}}}{C_\mu D_i}, \tag{9}$$

  where U_{in} and D_i denote the average inlet velocity and inner pipe diameter, respectively;
- the standard mass-conserving boundary condition was chosen at the outlet, with the pressure data specified according to measurements;
- adiabatic conditions were assumed at the outside pipe wall.

3.4 Validation of Pressure-Drop Predictions

In total, 28 TASCflow simulations were run to generate the data to be compared with measurements. Six simulations pertained to zero-power (adiabatic) conditions, and were used to validate pressure-drop predictions. The remaining simulations covered the full range of power and inlet conditions investigated experimentally, and were used primarily for validation of heat-transfer predictions.

An example of TASCflow-predicted pressure variation along the heated length of the 30%-obstructed channel is shown in Figure 7. The profile is compared with the corresponding experimental data obtained at the pressure taps, PT_2 and PT_3. The excellent agreement between the CFD-predicted and measured pressures, as shown in Figure 7, is typical of all high-flow cases studied. Understandably, due to higher experimental uncertainties associated with pressure measurement, the agreement between pressure-drop predictions and data was somewhat poorer for lower flow rates.

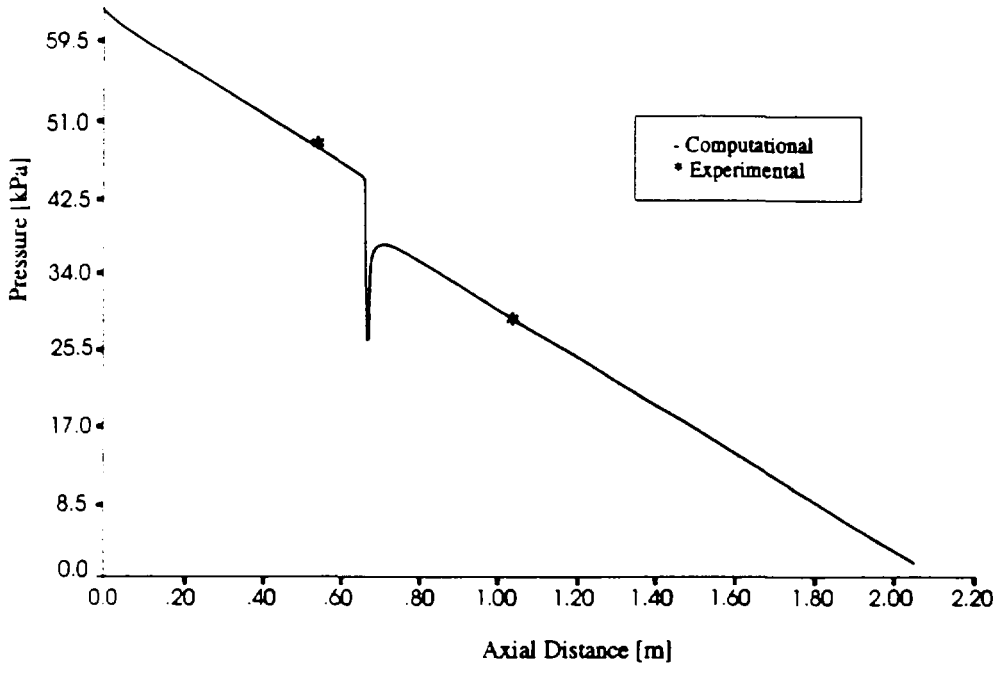

Figure 7: Sample Prediction of Axial Pressure Profile in 30%-obstructed Channel

As expected, equal pressure gradients were computed upstream and downstream of the obstruction in all cases. Analysis of TASCflow results has also confirmed that, for a given set of conditions, the same unit frictional losses were predicted in unobstructed, 17.8%-obstructed, and 30%-obstructed channels. This validation of frictional pressure losses was therefore limited to predictions of (*constant*) pressure gradients in bare channels, and they were found to be in good agreement with experimental data in all but the lowest-flow cases. Consequently, the reproduction of pressure measurements in obstructed channels could be viewed as a demonstration of the CFD-based methodology for accurate prediction of $K-factors$.

3.5 Validation of Heat-Transfer Predictions

A typical prediction of axial temperature profiles, extracted from one of the TASCflow simulations of the 30%-obstructed channel, is shown in Figure 8. As expected, at the entrance to the heated section, the outer- and inner-wall temperatures, T_{wo} and T_{wi}, and bulk fluid temperature, T_{bf}, were predicted to experience ramp changes, but they quickly adjusted to follow linear variations. The axial temperature gradients remained equal upstream and downstream of the ring obstruction, $dT_{wo}/dz \equiv dT_{wi}/dz \equiv dT_{bf}/dz$, but were clearly affected by the increased turbulence intensity in the recirculating flow regions behind the obstruction. In general, the outer-wall and fluid outlet temperatures were always satisfactorily predicted, considering the experimental uncertainty in estimating the power supplied to the test section.

A crucial component of this validation study was the comparison of predicted and measured changes of outer-wall temperatures downstream of the obstruction step. These changes were a direct measure of the intensity of heat-transfer promotion by turbulence in the downstream recirculation zone, and provided a stringent test for the versatility of k–ϵ turbulence modelling.

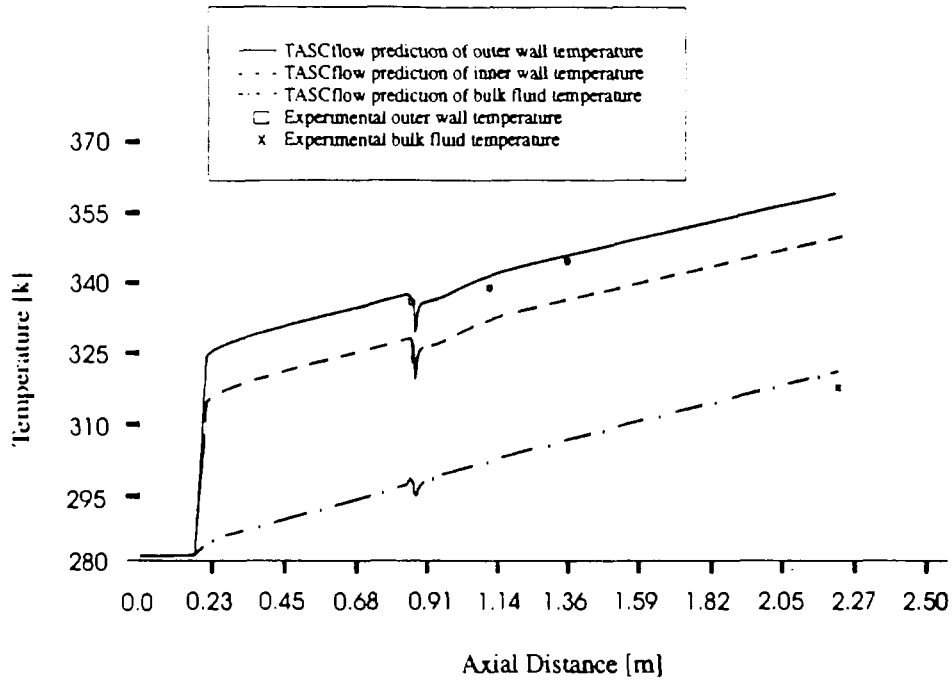

Figure 8: Sample Prediction of Wall- and Bulk-Temperature Profiles in 30%-obstructed Channel

Typical comparisons of predicted and measured temperature variations in this region are shown in Figures 9 and 10, for the 17.8% and 30% obstruction rings, respectively. The temperature changes were plotted over the axial distance of ~ 120 mm, starting at the location of each ring's downstream face. As demonstrated in Figures 9 and 10, CFD predictions captured the measured effects reasonably well, even though the fine details of predicted temperature variations could not be validated on the basis of the present measurements. Maximum departures from linear temperature profiles were predicted with quite well, indicating that heat-transfer enhancement by ring appendages could be correctly assessed on the basis of CFD simulations alone. While the detailed analyses of TASCflow simulation results are continuing, they are expected to shed more light on the effects of simplifying assumptions (listed in section 3.3) on the predictions of temperature-variation details downstream of appendages.

4 CONCLUSIONS AND FINAL REMARKS

- The effects of flow obstruction on heat transfer in single-phase flow and pressure drop were investigated experimentally in a directly heated tube of 8 mm ID, in Freon-134a. The obstructions used were rings that obstructed 17.8% and 30% of the flow areas.
- Numerical investigations of the same effects were pursued in parallel using the commercial CFD software, TASCflow. A 2-D finite-volume model of the test section was used to simulate turbulent flow and conjugated heat transfer in freon, pipe wall and ring material.
- The main experimental findings can be summarized as follows:
    1. Significant enhancement of wall-to-coolant heat transfer was observed in the experiments downstream of the flow obstruction. The enhancement was effective only over a

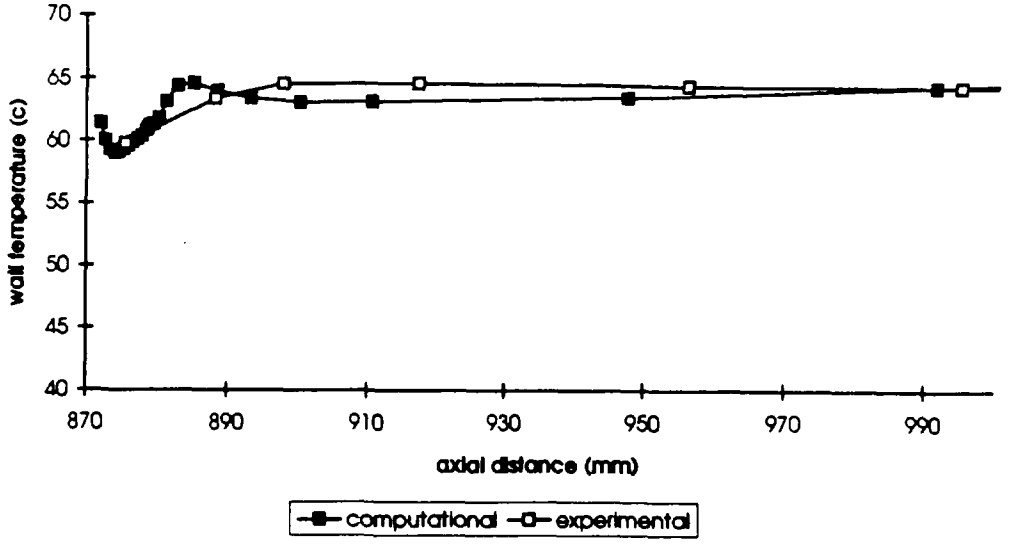

Figure 9: Example of Outer-Wall Temperature Variations Downstream of 17.8% Obstruction

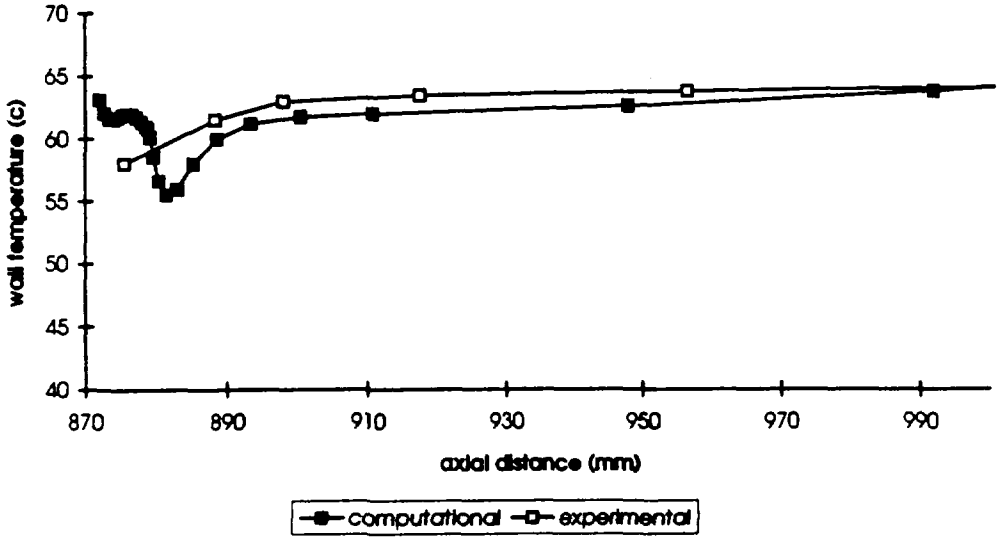

Figure 10: Example of Outer-Wall Temperature Variations Downstream of 30% Obstruction

short distance, and disappeared at $L/D_i \approx 5$ and $L/D_i \approx 10$, for the 17.8% and 30% obstruction rings, respectively.

2. The highest heat-transfer enhancement occurred at the lowest flow rate investigated. An increase in mass flux from 1000 to 6000 kg/m^{2}s weakened the heat-transfer enhancement at the same rate for both rings.
3. The pressure drop across the flow obstruction was measured and expressed in terms of the K-factor. The K-values of approximately 0.18 and 0.45 for the turbulent flow regime were derived for the rings 17.8% and 30%, respectively, and agree with those in the literature.

- All the experimentally observed dependencies were found to be quantitatively reproducible in CFD simulations using the *standard* k–ϵ model of turbulence. Pressure-drop predictions obtained with the TASCflow code were found to be in very good agreement with experimental data, and the code was shown to simulate the right trends in wall-temperature variations resulting from the proximity of channel obstructions. The predicted maximum temperature changes in the obstruction vicinity were in reasonable agreement with the measurements, revealing significant heat-transfer enhancement in vertical channels obstructed by cylindrical rings.
- The numerical study reported in this paper represents a contribution to the validation data bank of TASCflow software and its models. From a more general perspective, the quantitative agreement between CFD predictions and experimental data for ring-obstructed vertical tubes indicates viability of CFD-based assessment methodologies for applications to more complex channel geometries.

Acknowledgement. The work reported in this paper was supported by COG Working Party 7.

NOMENCLATURE

C_μ	empirical constant used to define eddy diffusivity in the k–ϵ model [–],
D	diameter [m],
D	diameter [m],
DC	direct current,
f	Fanning friction factor [–],
G	mass flux [kg/m^{2}s],
K	form-loss coefficient [–],
L	axial distance between the downstream face of obstruction ring and the thermocouple TCw_1 [m],
Nu	Nusselt number (based on hydraulic diameter) [–],
P	power to the test section [kW],
PC	power clamp,
Pr	Prandtl number [–],
PT	pressure transducer,
Δp	pressure drop [kPa],
Re	Reynolds number (based on hydraulic diameter) [–],
r	radius [m],

T	temperature [°C],
TC	thermocouple,
z	distance along axial direction [m].

Greek

γ	diffusivity [kg/(ms)],
Λ	Moody–Weisbach friction factor [–],
λ	thermal conductivity [W/(m·K)],
μ	viscosity [kg/(ms)],
ρ	fluid density [kg/m^3],
ϵ	turbulence dissipation rate [m^2/s^3].

Subscripts

bf	bulk fluid,
i	inner,
in	inlet conditions,
o	outer,
$obst$	flow with obstruction,
out	outlet conditions,
s	solid,
t	turbulent,
Tot	total,
$unobst$	unobstructed flow,
w	wall,
1, 2, 3	locations of thermocouples TCw_1, TCw_2, TCw_3.

REFERENCES

1. A.O. Banas, M.B. Carver, J.C.H. Leung and B.P. Bromley, "Multidimensional Simulations of Fuel-Rod Appendage Effects on Pressure Drop and Heat Transfer in an Annulus Flow", AECL report, AECL-10725 (1992).

2. A.O. Banas, M.B. Carver and C.A Whitehead, "Numerical Studies of Flow and Heat Transfer around CANDU Fuel–Element Bearing Pads", Proc. Fourth Intern. CNS/ANS Conf. on Simulation Methods in Nuclear Engineering, Montreal, Quebec (1993).

3. AEA Technologies, "CFDS-FLOW3D, Release 3.3" (1994).

4. Advanced Scientific Computing Ltd., "TASCflow3D, Version 2.3" (1994).

5. I.K. Idelchik, "Handbook of Hydraulic Resistance", pp. 145-171, Second Edition, Hemisphere Publishing Corporation (1986).

6. B.E. Launder and D.B. Spalding, "The Numerical Computations of Turbulent Flows", *Comp. Meth. Appl. Mech. Engng.* **3** (1974) 269.

ASSERT Software Quality Assurance, Benchmark Testing and Parametric Studies

J.C. Kiteley, M.B. Carver, G.M. Waddington and S.V. Junop

Fuel Channel Thermalhydraulics Branch
Atomic Energy of Canada Limited
Chalk River Nuclear Laboratories

ABSTRACT

This paper gives a brief introduction to the ASSERT subchannel code and outlines the software quality assurance (SQA) protocol and source code management (SCM) system for code development in a team environment. The acceptance criteria or benchmark database for the ASSERT code is presented; that allows for qualitative verification of the code over a wide range of conditions and solution options, and ensures that our successive code production versions meet our SQA standard before being released.

Examples of the use of ASSERT for parametric studies or sensitivity analysis are given to illustrate how the code can be used to examine the separate effects of fuel channel geometry, boundary conditions, and sub-model options. Specific examples are also given showing the sensitivity of the ASSERT code to the use of the CHF table look-up method and its various correction factors, transient CHF analysis and numerical experiments to investigate the separate sub-models of the advanced drift flux model in ASSERT.

The purpose of this paper is to present a pragmatic method of software quality assured code development and to illustrate how a subchannel analysis code may be used for various applications and to analyze the sensitivity of fuel channel conditions to separate effects. Conclusions and future directions for the ASSERT code are presented.

19th Annual Nuclear Simulation Symposium
Canadian Nuclear Society
McMaster University
Hamilton, Ontario.

October 15-17, 1995